LIPID SIGNALING

Distinct Signaling Roles of Ceramide Species in Yeast Revealed Through Systematic Perturbation and Systems Biology Analyses

David J. Montefusco,[1]* Lujia Chen,[2]* Nabil Matmati,[1,3] Songjian Lu,[2] Benjamin Newcomb,[1,3] Gregory F. Cooper,[2] Yusuf A. Hannun,[1,3]† Xinghua Lu[2]†

Ceramide, the central molecule of sphingolipid metabolism, is an important bioactive molecule that participates in various cellular regulatory events and that has been implicated in disease. Deciphering ceramide signaling is challenging because multiple ceramide species exist, and many of them may have distinct functions. We applied systems biology and molecular approaches to perturb ceramide metabolism in the yeast *Saccharomyces cerevisiae* and inferred causal relationships between ceramide species and their potential targets by combining lipidomic, genomic, and transcriptomic analyses. We found that during heat stress, distinct metabolic mechanisms controlled the abundance of different groups of ceramide species and provided experimental support for the importance of the dihydroceramidase Ydc1 in mediating the decrease in dihydroceramides during heat stress. Additionally, distinct groups of ceramide species, with different *N*-acyl chains and hydroxylations, regulated different sets of functionally related genes, indicating that the structural complexity of these lipids produces functional diversity. The transcriptional modules that we identified provide a resource to begin to dissect the specific functions of ceramides.

INTRODUCTION

Ceramides constitute a family of structurally related molecules that form the core structure of the broader family of bioactive lipids found in all eukaryotes, the sphingolipids (*1*). These structural variants of ceramide arise from the condensation of one or more sphingoid bases and several fatty acids. These, in turn, can be modified by the addition of distinct hydroxyl groups on either the sphingoid backbone or the fatty acid. Thus, the biosynthesis of ceramides is the product of the combinatorial action of multiple enzymes that control the structural variations of the ceramide products. In yeast (*Saccharomyces cerevisiae*), ceramide biosynthesis (Fig. 1) generates more than 30 distinct species that can be identified by contemporary mass spectroscopy–based lipidomic approaches (*2*); in mammals, the total number of ceramide species may exceed 200 (*3*).

In humans, ceramides are collectively involved in physiological processes, such as growth regulation and apoptosis, and in pathological conditions, such as diabetes and cancer (*2*). However, a fundamental question of ceramide-mediated signaling is whether the structural diversity of ceramides underlies functional diversity. That is, do the distinct ceramides encode specific signals? Although manipulation of individual enzymes of ceramide metabolism has enabled assignment of specific functions to these enzymes (*1*, *4*, *5*), these approaches do not clearly delineate the specific lipid species involved in the process, because sphingolipid metabolism constitutes a highly connected network such that perturbing the function of an enzyme can lead to broad changes in sphingolipid species beyond the substrates and products of the enzyme (metabolic ripple effects) (*3*, *6*). Pinpointing the functions of the lipid or lipids implicated by manipulating a sphingolipid metabolic enzyme is critical in deciphering the specific downstream pathways and the mechanisms that mediate the changes in cellular behavior, because it is the lipid product and not the enzyme per se that propagates the downstream signal. Therefore, new tools and approaches capable of delineating connections between specific ceramide structures and diverse downstream signaling pathways are needed.

S. cerevisiae has emerged as a powerful model to dissect metabolic and functional pathways of sphingolipids. Activation of de novo sphingolipid synthesis is essential for yeast to survive heat stress (*7*, *8*), and sphingolipids mediate specific downstream processes in response to heat stress, such as cell cycle arrest (*9*–*11*), mRNA sequestration (*12*), and inhibition of nutrient uptake (*13*). Microarray analysis revealed that de novo synthesis of sphingolipids mediates the regulation of several hundred genes in response to heat stress (*14*). This simultaneous sphingolipid-dependent regulation of diverse processes provides an opportunity to identify functions of diverse ceramide species, but also requires the development and application of novel methodology.

RESULTS

Systematic perturbation of sphingolipid metabolism decouples the biosynthesis of some groups of lipids

Our overall framework of dissecting the functions of specific ceramide species in yeast proceeded as follows: (i) systematically perturb ceramide metabolism using physiological and pharmacological treatments, (ii) monitor lipidomic and transcriptomic responses to the treatments, and (iii) apply systems biology analysis to deconvolute the signaling roles of ceramide species in these responses. Yeast cells were subjected to different combinations (see Materials and Methods for details) of heat stress, ISP1 (myriocin)

[1]Department of Biochemistry and Molecular Biology, Medical University of South Carolina, Charleston, SC 29445, USA. [2]Department of Biomedical Informatics, University of Pittsburgh, Pittsburgh, PA 15232, USA. [3]Department of Medicine and the Stony Brook Cancer Center, Stony Brook University, Stony Brook, NY 11794, USA.
*These authors contributed equally to this work.
†Corresponding author. E-mail: yusuf.hannun@stonybrookmedicine.edu (Y.A.H.); xinghua@pitt.edu (X.L.)

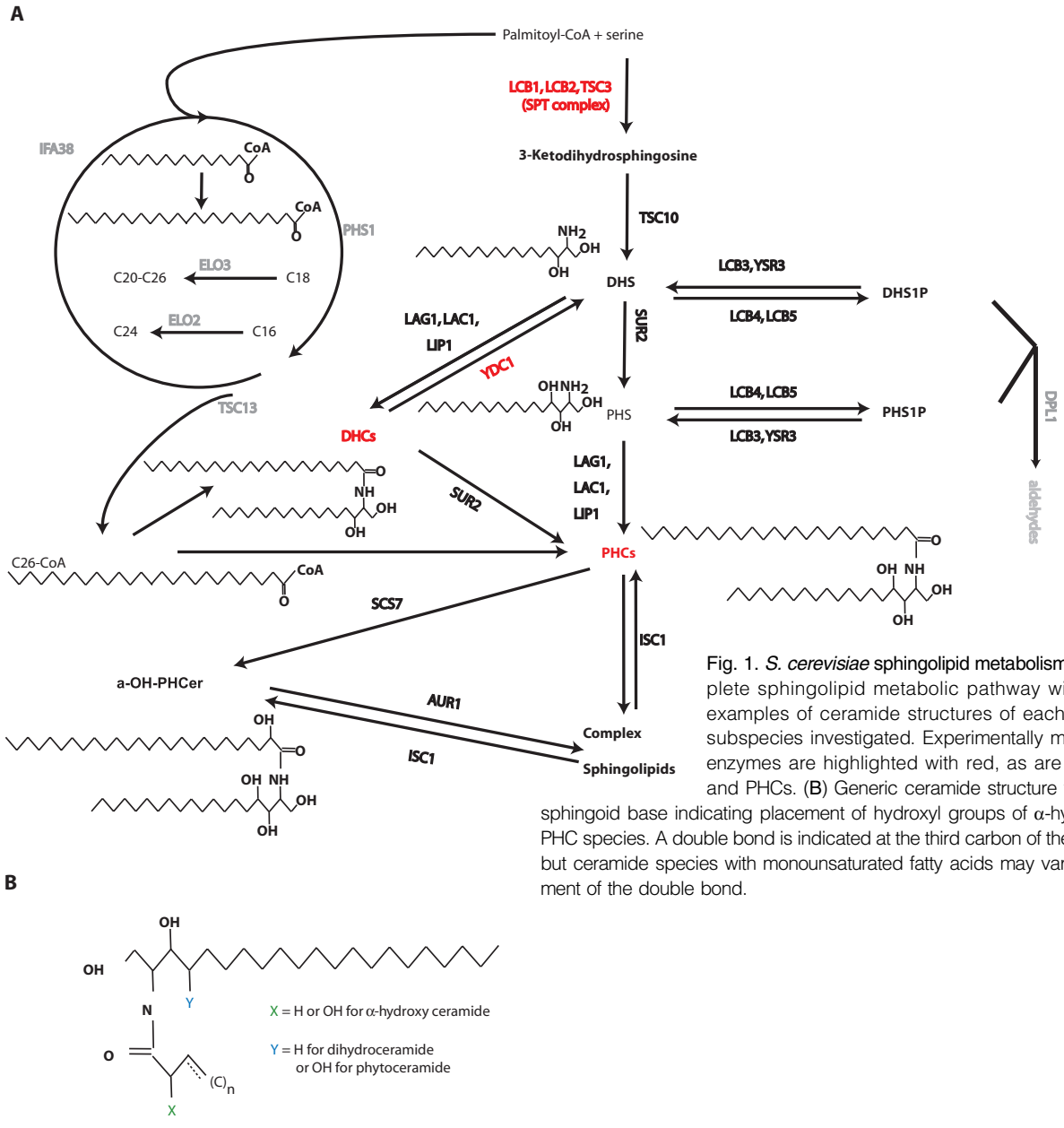

Fig. 1. *S. cerevisiae* sphingolipid metabolism. (A) Complete sphingolipid metabolic pathway with explicit examples of ceramide structures of each ceramide subspecies investigated. Experimentally manipulated enzymes are highlighted with red, as are the DHCs and PHCs. (B) Generic ceramide structure with a C18 sphingoid base indicating placement of hydroxyl groups of α-hydroxy and PHC species. A double bond is indicated at the third carbon of the fatty acid, but ceramide species with monounsaturated fatty acids may vary in placement of the double bond.

treatment, and myristate treatment (Fig. 2A), with each perturbation affecting different part(s) of the lipid metabolic network and leading to diverse lipid profiles. We measured the relative abundance of the ceramide species by mass spectrometry and the changes in gene expression in response to these perturbations using microarrays (Fig. 2B). We then performed a systems biology analysis to identify correlated changes in ceramide species and gene expression and identified lipid groups that showed similar profiles under all perturbations (Fig. 2C). Using ontology-based functional analysis and transcription factor analysis (Fig. 2, D and E), we identified functional modules among the genes that were potential targets regulated by a specific ceramide species (or a lipid group). Selected predicted functional associations were validated using phenotypic and transcriptomic experiments (Fig. 2F).

We first studied ceramide profiles when cells were subjected to heat stress and investigated the impact of blocking de novo synthesis using ISP1, which inhibits the serine palmitoyltransferase (SPT) complex (Fig. 1), the first committed reaction in the de novo pathway of sphingolipid biosynthesis. Many ceramide species, especially the phytoceramide family (PHC), responded to heat stress through increased de novo synthesis (Fig. 3A and table S1). These included C14, C16, and C18 PHC and α-hydroxy–PHCs (as an example, see inset in Fig. 3A for C14–α-hydroxy–PHC). In contrast, several members of the dihydroceramide family (DHC) such as saturated C24 and C26 DHC decreased during heat stress in the presence or absence of ISP1 (Fig. 3A). The decrease of DHCs during heat stress is a novel finding, and the mechanism of how heat stress affects these species has therefore not been defined.

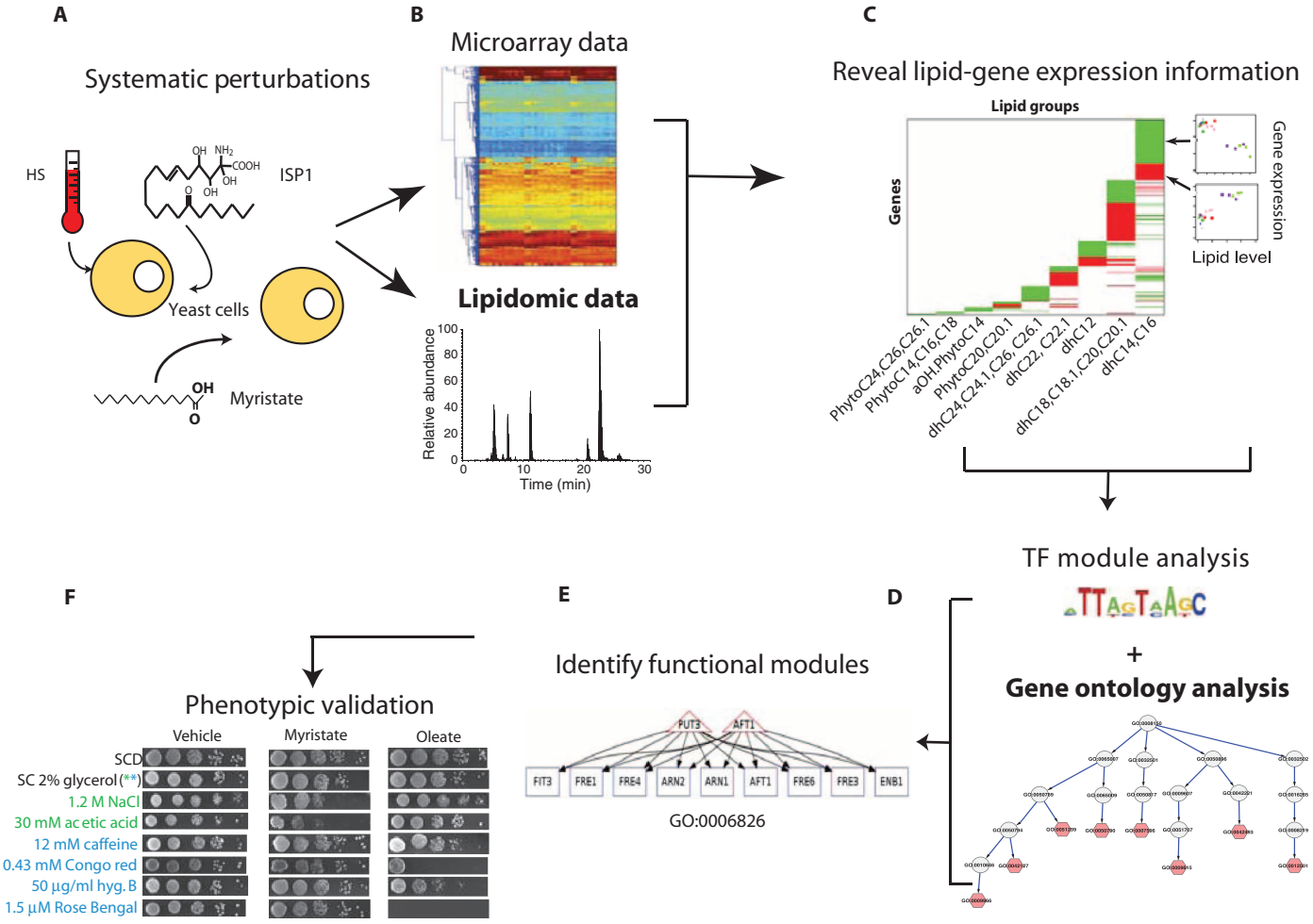

Fig. 2. Overall strategy of the study. (A) Perturbing sphingolipid metabolism in different experimental conditions: heat stress (HS), ISP1, and myristate treatments. (B) Collecting lipidomic and gene expression (microarray) data. (C) Modeling the relationship between lipids and genes. The pseudocolored matrix shows that different lipid groups (columns) are significantly correlated with different genes (rows). The scatter plots illustrate that genes in the green region of the matrix are negatively correlated with a lipid and that those in the red region are positively correlated with a lipid. (D) Performing ontology-based function analysis and transcription factor (TF) analysis. (E) Identifying functional modules associated with lipid groups. Triangles represent genes encoding transcription factors, rectangles depict genes, and an edge indicates that a gene is regulated by a transcription factor. (F) Validating prediction using phenotypic assays. hyg. B, hygromycin B.

To test the hypothesis that different ceramides regulate distinct cellular signals to mediate cell stress responses, we sought to infer the signaling roles of different ceramide species using gene expression data as readouts of cellular signals. Because of the high connectivity of the sphingolipid metabolic network (*6*), many species, for example, DHCs differing only in *N*-acyl chain length, showed correlated changes during heat stress (Fig. 3A), which obscured potential contributions of individual ceramides or subsets of ceramides. To further dissect and segregate specific ceramide responses, we treated cells with the fatty acid myristate, coupled with treatment with ISP1, to define more specific ceramide responses.

Fatty acid treatment changes the concentration of lipid species with a particular fatty acid side chain (*15*–*17*). Matmati *et al.* showed that adding different fatty acids with different chain lengths to the medium enriches the PHC pool with those PHC species that correspond to the same chain length (*18*). Using this methodology, we treated yeast cells with the long-chain (C14) fatty acid myristate to trigger an acute increase of ceramides with the corresponding C14 acyl chains. Additionally, we also treated the cells with ISP1 to block the incorporation of myristate or palmitate (derived from myristate elongation) into the sphingoid backbone, which would lead to an indiscriminate increase in sphingolipids. Upon myristate treatment, C14, C16, and C24 DHC and C14 PHC species increased (Fig. 3B). Moreover, several other ceramide species (Fig. 3B) and the sphingoid bases (C0) (fig. S1 and table S1) decreased in response to myristate, suggesting selective channeling of sphingoid bases to C14 DHC and C14 PHC at the expense of other ceramides. Thus, the C14 and C16 ceramides were effectively decoupled from other ceramides, creating a contrast that would help to resolve the signaling role of these species from other ceramides.

To reveal biologically meaningful patterns from the complex lipidomics data sets collected from the systematic perturbations, we applied consensus clustering analysis (*19*, *20*) to the pooled lipidomic data sets to identify

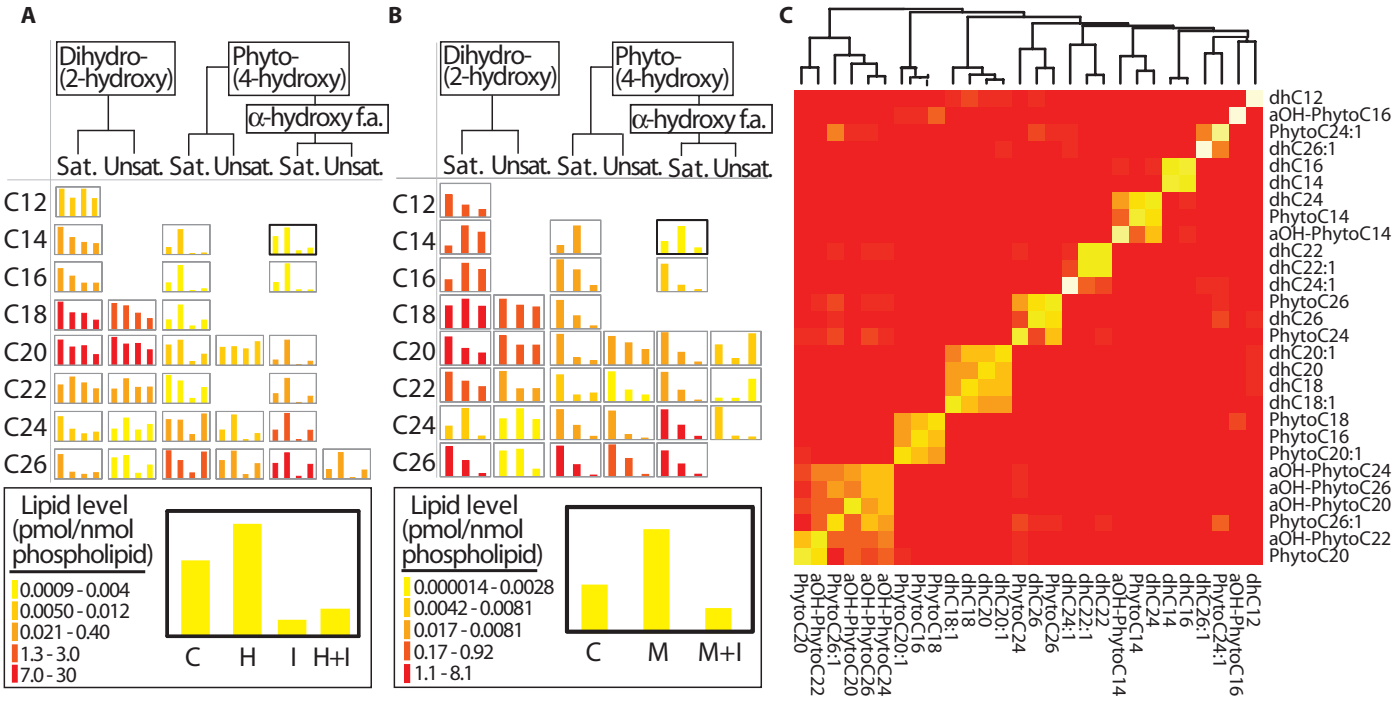

Fig. 3. Lipidomic analysis. (A) Lipidomic response to combinations of heat stress and ISP1 treatment. Control (C), heat (H), ISP1 (I), and heat plus ISP1 (H+I). (B) Lipidomic response to combinations of myristate and ISP1 treatment. Control (C), myristate (M), and myristate plus ISP1 (M+I). In (A) and (B), rows represent *N*-acyl chain length, and columns represent single combinations of hydroxyl groups for each ceramide. Saturated (Sat.) and monounsaturated (Unsat.) *N*-acyl chains are indicated. Bar height is averaged triplicate ceramide abundance; the range of each chart is color-coded. Legend inset: C14–α-hydroxy–PHC. (C) Consensus clustering of lipidomic data. The heat map of the consensus matrix reflects how frequently a pair of lipids is assigned to a common cluster during repeated sampling and clustering. A red cell in the matrix indicates that a pair of lipids tends to be assigned to mutually exclusive clusters, and a yellow cell indicates that a pair tends to be assigned to a common cluster. Lipid name abbreviations: dh, dihydro; aOH, α-hydroxy; C followed by a number, fatty acid chain length. See table S1 for lipid mass spectrometry data.

distinct lipid groups. The consensus clustering method repeatedly performs clustering among randomly drawn subsets of the samples to identify intrinsic subgroups of samples, in the current case, the lipids that were inseparable during the repeated clustering. The results showed that ceramides could be further segregated into distinct subgroups (the yellow blocks in Fig. 3C), identifying lipid subgroups, such as one containing C16, C18, and C20.1 PHCs and one containing C18 and C20 DHCs (Fig. 3C). Generally, the lipid species that cosegregated into individual ceramide clusters share similar structures and are mostly products of a common set of specific enzymatic reactions in the sphingolipid pathway. For example, the cluster consisting C16, C18, and C20.1 PHCs is separated from the cluster composed of C18, C18.1, C20, and C20.1 DHCs, and synthesis of these ceramide species is metabolically separated by the function of the hydroxylase, Sur2. Clear separation of these clusters indicated that the perturbations induced distinct profiles and decoupled lipids that would exhibit a similar profile if the yeast had only been exposed to a single perturbation, for example, heat stress.

On the basis of the results of clustering analysis and knowledge of ceramide metabolism, we divided the ceramides into nine major groups (table S2), within which group members were statistically inseparable in the clustering analysis and metabolically inseparable based on biosynthetic pathways. Identification of these clusters lends credence to the theory that enzymes in the sphingolipid metabolism network respond to cellular changes, thus producing distinct profiles for different species. Therefore, we hypothesized that each group functions as a single metabolic, signaling, and functional unit and attempted to identify their corresponding downstream targets using gene expression data and statistical analyses.

Transcriptomic responses are specific to perturbations in sphingolipid metabolism

From the microarray data collected in parallel to the lipidomic data, we identified differentially expressed genes responding to different perturbations (Fig. 4A and table S3). We identified 1893 lipid-mediated stress-responding genes that represented the intersections of the heat-sensitive genes with the ISP1-sensitive and with the myristate-sensitive genes. The members of the union gene set were ISP1-sensitive and thus dependent on de novo synthesis of sphingolipids, corroborating previous findings that sphingolipids play an important role in the yeast stress responses (*21–24*).

To test the hypothesis that distinct ceramides encode disparate signals, which can be detected through the regulation of distinct target gene sets, we studied the relationship between lipidomic and transcriptomic data using three distinct methodologies: (i) the maximum information coefficient (MIC) (*25*), (ii) the Pearson correlation analysis, and (iii) a Bayesian regression model. The MIC quantifies the information between a pair of variables, such as a lipid species profile and a gene expression profile. MIC can capture both linear and nonlinear relationships between variables in a form similar to the familiar correlation coefficient, although the measured association (positively or negatively associated) lacks directionality.

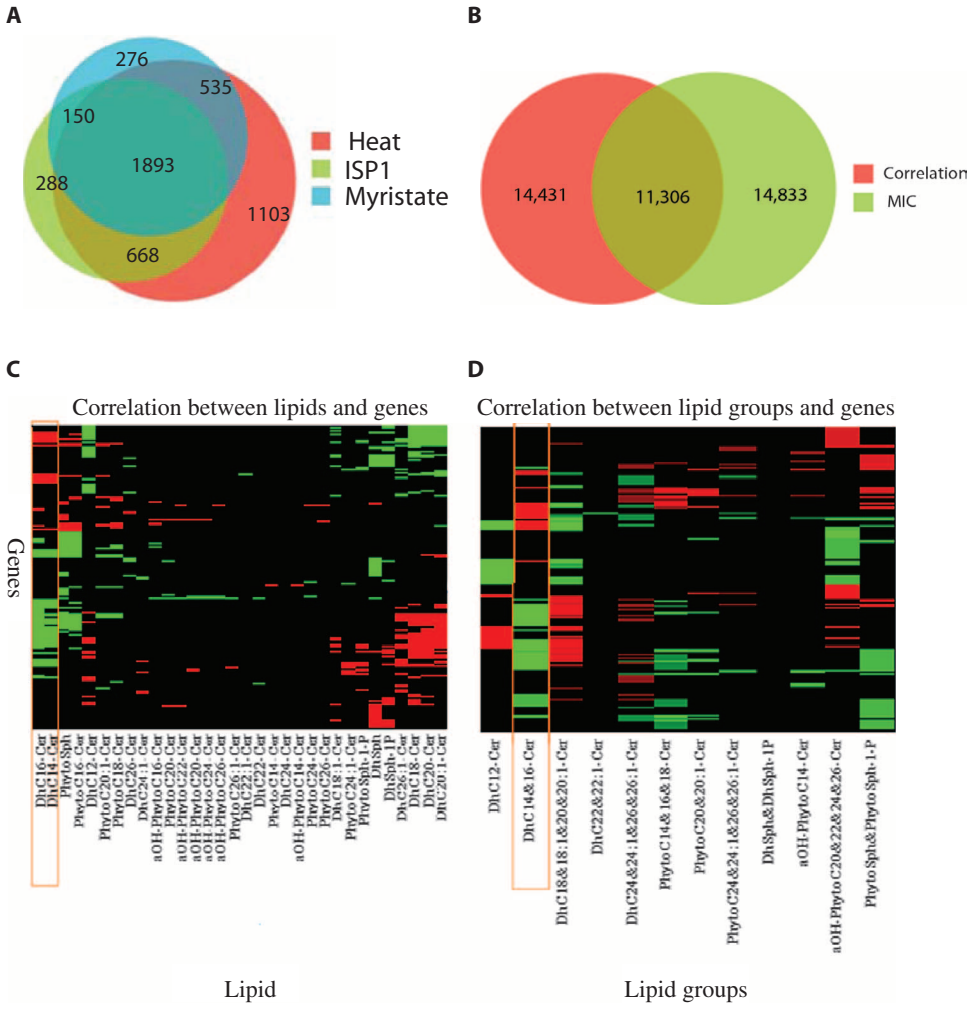

Fig. 4. Assessing the correlation between lipid abundance and gene expression. (A) Venn diagram illustrating number of genes sensitive to different treatments. (B) Venn diagram illustrating number of lipid-gene pairs with significant association assessed using MIC and Pearson correlation analyses. (C and D) Heat map representation of Pearson correlation coefficient between lipids (C) or lipid groups (D) and gene expression. In the figures, rows correspond to genes that have significant correlation with at least one lipid species, and columns correspond to lipid species. In both figures, a black cell indicates that the corresponding lipid-gene pair is not significantly correlated; a red cell represents that the pair is positively correlated; and a green cell indicates positively that the pair is negatively correlated. Left panel shows the correlation of genes with respect to all lipid species; right panel shows the correlation of genes with respect to lipid groups. See table S3 for microarray data.

We assessed the significance of MIC and the Pearson correlation of all lipid-versus-gene pairs. A total of 26,139 lipid-gene pairs had significant MIC values ($P < 0.01$; Fig. 4B); 25,737 lipid-gene pairs had significant Pearson correlation coefficients ($P < 0.01$) with a false discovery threshold q value (*26*) set at $q < 0.05$. There were non-overlapping portions of the MIC (table S4) and Pearson sets (table S5), which likely reflect the difference in assessing statistical significance between the two methods (Fig. 4B). We also performed a series of permutation tests in which lipidomic data were randomly permuted to assess the false discovery rate (*27*). None of the Pearson correlation coefficients derived from the permutation experiment passed the threshold of $P < 0.01$ and $q < 0.05$, indicating that the observed relationships between lipids and gene expression were not false discoveries that could result from multiple statistical testing. By Pearson analysis, we identified genes that exhibited a significant correlation, either positive or negative, with at least one lipid species (Fig. 4C), and clusters of similarly regulated genes were apparent when the correlations were performed on lipid groups (Fig. 4D and table S5).

For the third method, we used a regularized regression model (*28*), which represents the expression value ($\log_2$-based) of a gene as a linear function of lipids. It progressively shrinks the weighting coefficient of each lipid predictor toward zero if that predictor is not statistically associated with the gene expression, until leaving only a single predictor with a nonzero coefficient. With this model, we achieved the following goals: (i) identifying the most informative ceramide with respect to a gene, (ii) representing the direction of a lipid influence (stimulate or inhibit), and (iii) providing a mathematical means to predict gene expression as a function of lipid concentration (Fig. 5A and table S6). We pooled the genes potentially regulated by each lipid cluster and further grouped them according to the direction of regulation (Fig. 5A). Each ceramide group had statistically significant parameters with respect to a set of genes, and the gene sets associated with different ceramides were largely non-overlapping, thus supporting the hypothesis that each species plays roles in distinct pathways regulating different gene sets. We also noticed that distinct gene sets were associated with ceramides with the same head group but different acyl chain lengths, for example, those associated with long-chain (C14 and C16) DHCs were different from those associated with very long chain (C18, C18.1, C20, and C20.1) DHCs (referred to as LC-DHCs and VLC-DHCs, respectively).

To better define ceramide-dependent biological processes and to provide mechanistic understanding of ceramide-specific pathways, we performed ontology-based, semantic-driven function analysis and transcription factor analysis of potential target genes. We divided the genes significantly associated with a lipid group into modules (certain genes can be in more than one module) by mining their Gene Ontology (GO) annotations (*29*), such that each module contains genes that participate in coherently related biological processes, which can be encompassed by a GO term that retains as much of the semantic meaning of their original annotations as possible. Figure 5A illustrates that a module of genes involved in the biological process iron ion transportation (GO:0006826) and another module of genes involved in vacuolar protein catabolic process (GO:0007039) were found among the genes negatively correlated to LC-DHCs and VLC-DHCs, respectively.

We then applied a graph-based algorithm to search for a set of transcription factors that regulate the members of a module in a cooperative fashion, thus producing a transcription factor module. The analyses, as illustrated by the examples in Fig. 5B, revealed that the genes in these modules not only performed related functions but also shared transcription factors, which provided mechanistic evidence that the genes in a module were regulated by a common signal. Our functional analyses project the molecular findings from a gene level onto a conceptual level. For example, the results in Fig. 5B can be translated into the following prediction: "LC-DHCs regulate the genes involved in iron ion transportation." Thus, these gene modules produce testable hypotheses regarding functions of specific groups of ceramide species. All gene modules identified by our analyses—a function map of the ceramide-dependent genes—are available at the Web site http://www.dbmi.pitt.edu/publications/YeastCeramideSignaling. Note that not all modules have transcription factors associated with them because of limitations in the available data regarding gene promoters and their regulatory transcription factors.

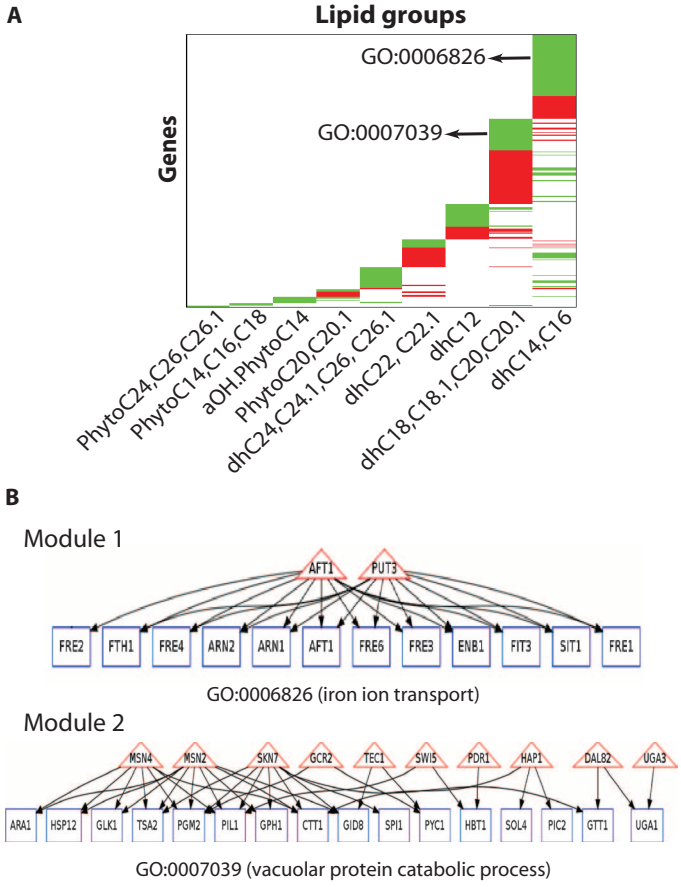

Fig. 5. Modeling relationship between lipidomic and gene expression data. (A) Organizing genes demonstrating significant correlation with specific ceramides. Genes (rows) are organized according to their association with the different lipid subgroups. A green block represents a set of genes negatively correlated to a lipid, and a red block represents a set of genes positively correlated to a lipid. Examples of major enriched GO terms within gene blocks are shown. (B) Defining pathways of specific biologic modules that respond to specific ceramides, perform related functions, and share transcription factors. Two example modules are shown (see http://www.dbmi.pitt.edu/publications/YeastCeramideSignaling for all modules). Rectangles represent lipid-correlated genes, triangles indicate the transcription factors shared by the genes, and an edge from a transcription factor to a gene indicates that the gene has the binding sites for the transcription factor in its promoter. The function performed by the genes in a module is represented with a GO term.

Heat stress affects DHC metabolism through activation of Ydc1

Heat stress resulted in a decrease in several DHCs through a mechanism that was not inhibited by ISP1 and thus did not require de novo synthesis of sphingolipids (Fig. 3A). In turn, these changes in DHCs affected the expression of a large number of genes (Fig. 5A), reflecting their important role in mediating the cellular response to heat stress. Therefore, we investigated the molecular mechanism through which heat stress

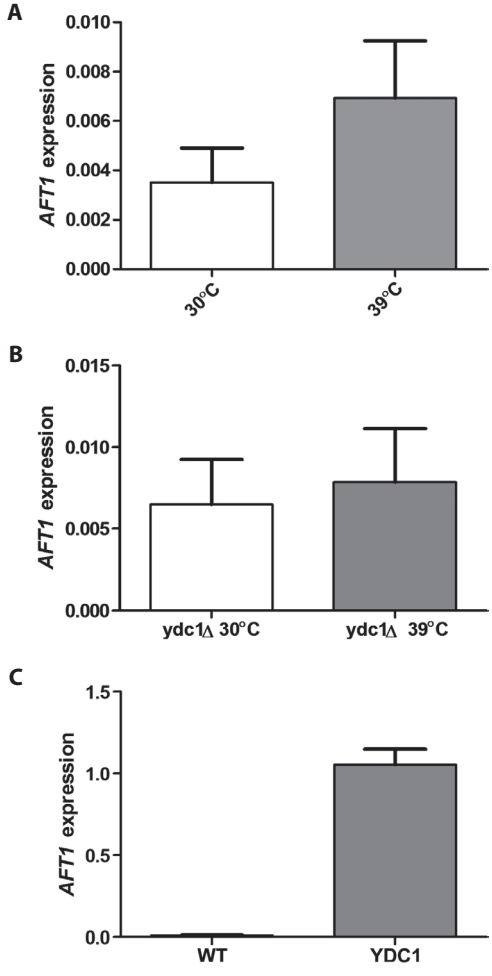

Fig. 6. Role of Ydc1 in mediating the impact of heat stress on gene expression. (A) Effect of heat stress on *AFT1* expression in wild-type (WT) yeast cells (n = 6 and 4, for 30° and 39°C, respectively). (B) Effect of heat stress on *AFT1* expression in the *ydc1*Δ strain (n = 4, for 30° and 39°C). (C) Effect of overexpression of *YDC1* on *AFT1* expression at 30°C (n = 6 and 2, for WT and +*YDC1*, respectively). Data are shown as means ± SE except for in (C), where the data are shown as average and half of the range for the two +*YDC1* measurements.

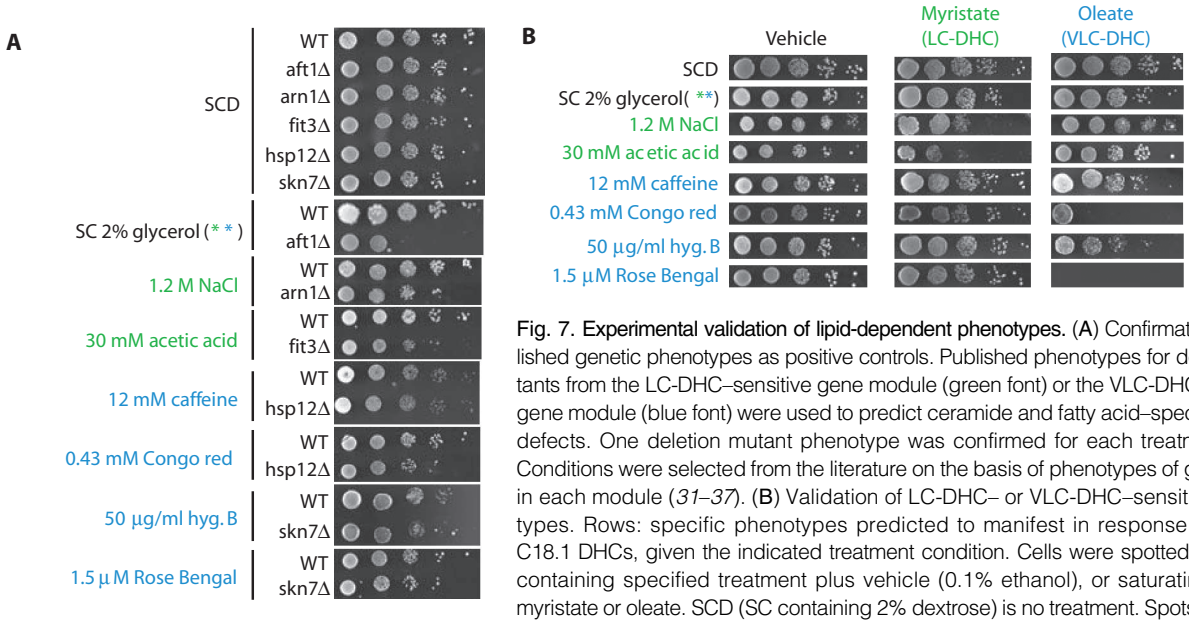

Fig. 7. Experimental validation of lipid-dependent phenotypes. (**A**) Confirmation of published genetic phenotypes as positive controls. Published phenotypes for deletion mutants from the LC-DHC–sensitive gene module (green font) or the VLC-DHC–sensitive gene module (blue font) were used to predict ceramide and fatty acid–specific growth defects. One deletion mutant phenotype was confirmed for each treatment used. Conditions were selected from the literature on the basis of phenotypes of genes within each module (*31*–*37*). (**B**) Validation of LC-DHC– or VLC-DHC–sensitive phenotypes. Rows: specific phenotypes predicted to manifest in response to C14 or C18.1 DHCs, given the indicated treatment condition. Cells were spotted onto agar containing specified treatment plus vehicle (0.1% ethanol), or saturating (1 mM) myristate or oleate. SCD (SC containing 2% dextrose) is no treatment. Spots represent 1:10 serial dilutions of a single mid-log culture. Green font: phenotypes of the LC-DHC–sensitive module predicted to be induced by myristate treatment. Blue font: phenotypes of the VLC-DHC–sensitive module predicted to be induced by oleate treatment, and 2% glycerol is associated with both modules. Images are representative of triplicate experiments (fig. S2).

affected DHC metabolism, more specifically to identify the enzyme(s) that mediates the effect of heat stress.

The alkaline dihydroceramidase (encoded by the *YDC1* gene) is a good candidate enzyme to mediate the impact of heat stress on long-chain DHCs. Ydc1 hydrolyzes DHCs preferentially over PHCs (*30*) to a free fatty acid and dihydrosphingosine, thus reducing the concentration of all DHCs. Aft1 is one of the transcription factors associated with the LC-DHC negatively correlated genes, and the *AFT1* gene is in the gene module, thus forming a positive feedback loop. Therefore, we analyzed the expression of *AFT1* as an indicator of the transcriptional activity of Aft1 in the *YDC1* deletion and overexpression yeast strains. We measured *AFT1* expression to assess whether Ydc1 was required to mediate changes in gene expression in response to heat stress (Fig. 6, A and B). Heat stress–induced *AFT1* expression (Fig. 6A) and deletion of *YDC1* attenuated the response (Fig. 6B). Overexpression of *YDC1* should decrease DHCs and, thus, mimic the reduction in DHCs caused by the heat stress. Strikingly, overexpression of *YDC1* induced *AFT1* more than a hundredfold compared with that in wild-type yeast (Fig. 6C). Thus, our results confirmed that DHCs regulated the expression of *AFT1* in module 1, and Aft1 is likely involved in this response. The results also indicated that activation of Ydc1 is sufficient to induce gene expression changes similar to those induced by heat stress; thus, it is likely one of the enzymes that mediate the impact of heat stress on DHC metabolism.

Phenotypic experiments validate distinct signaling roles of different DHCs

The integrative analyses of lipidomic and transcriptomic data led to the following hypothesis: DHC species with different side chains participate in different signaling pathways. To investigate whether specific transcriptional regulations by distinct DHCs had functional impacts on cells, we examined the effects of perturbing DHCs on cell phenotypes. We focused on the two gene modules shown in Fig. 3C, which are suggested to be regulated distinctly by LC-DHCs or VLC-DHCs. Because these modules were negatively correlated with the specific DHC groups, we predicted that increasing the respective lipids would repress genes in the corresponding modules and would produce phenotypes mimicking those resulting from deletion of module genes. We identified 17 phenotypes associated with deletion of the genes in the two modules (table S7), and we then evaluated yeast cell growth after treatment with myristate or oleate to increase production of the LC-DHCs and VLC-DHCs, respectively.

We analyzed in detail seven phenotypes on the basis of deletion mutant phenotypes (*31*–*37*) for the genes within the LC-DHC–sensitive gene module or the VLC-DHC–sensitive gene module (Fig. 7A). For example, the genes *ARN1*, *ARN2*, and *FRE3* were among iron transport genes that should be negatively regulated by LC-DHCs as predicted by our analysis (Fig. 5B), and their corresponding deletion mutant strains *arn1*Δ, *arn2*Δ, and *fre3*Δ are all sensitive to high sodium. Increased production of LC-DHCs by myristate treatment, but not increased VLC-DHCs induced by oleate treatment, reproduced this growth defect in the wild-type strain (Fig. 7B and fig. S2). Conversely, increased production of VLC-DHCs by oleate treatment, and not by myristate treatment, reproduced the Congo red and Rose Bengal sensitivity phenotypes associated with *HSP12* and *SKN7* deletions (*35*, *37*), respectively. We expected that oleate and the corresponding increase in VLC-DHCs would mimic the phenotypes of *hsp12*Δ because this gene was identified from the microarray data as negatively correlated with VLC-DHCs. Skn7 is a transcription factor required to induce the genes involved in oxidative responses, and a profound sensitivity of *skn7*Δ to the singlet oxygen–producing chemical Rose Bengal was reported (*37*). Our transcription factor analysis indicated that Skn7 likely stimulates the transcription of seven genes in module 2, thus leading to the hypothesis that VLC-DHCs regulate these genes through suppression of the transcriptional activity of Skn7. Oleate treatment led to a marked increase in sensitivity to Rose Bengal in wild-type cells in a lipid-specific manner, which is consistent with the hypothesis that VLC-DHCs inhibited the transcriptional activity of Skn7. The results from these phenotypic experiments demonstrate the identification of specific functional responses to specific groups of ceramides.

DISCUSSION

Here, we addressed the challenging task of determining specific signaling roles of distinct ceramides in yeast. In general, a well-established approach to infer causal relationship between two objects (or events) is to manipulate the potential causal object (or event) in a random trial while investigating whether the target object (or event) consistently responds to such manipulations (*38*). Adopting this principle to lipid-mediated signaling, we applied a series of perturbations to manipulate sphingolipid metabolism, with each leading to unique changes in both ceramide metabolism and gene expression through distinct mechanisms. The results showed significant correlations (linear or nonlinear) between specific ceramide species or ceramide groups and gene expression despite the diversity of lipid and gene response to these perturbations, thus supporting the hypotheses that causal relationships exist between the ceramides and genes studied in this report. Although it is possible that each perturbation may exert effects on gene expression (or phenotypes) through additional confounding mechanisms other than through ceramides, systematic perturbation experiments reduced the likelihood of such effects. For example, the combination of multiple approaches to manipulate LC-DHC—reducing these lipids by heat stress, myrocin treatment, or overexpression of *YDC1*, and inducing these lipids by myristate treatment—effectively minimizes the impacts of potential confounding factors associated with each individual manipulation. Thus, we confidently concluded that LC-DHCs regulated the genes in module 1.

In conclusion, ceramides mediated a multitude of distinct cellular signals in the yeast stress responses. Additionally, this study revealed that the abundance of DHCs was decreased during the yeast response to heat stress, likely through activation of the dihydroceramidase (Ydc1). Functionally, the various DHCs regulated distinct subsets of target genes predicted to participate in distinct biologic processes. Overall, we provided evidence that distinct ceramide species with different *N*-acyl chains, functional groups, and hydroxylation participate in regulatory processes. The structural complexity of ceramides underscores the potential diversity of the functions that they can play in cellular systems because even closely related ceramides (such as LC-DHCs versus VLC-DHCs) regulated distinct sets of functionally related genes. These findings suggest new research directions in the study of ceramide-mediated signaling, including their roles in human physiology and disease.

MATERIALS AND METHODS

Yeast strains and culture conditions

Yeast strains used in this study including genotypes are listed in table S8. YPD (yeast extract, peptone, and dextrose) medium was used for the heat stress experiment, and for fatty acid treatment, synthetic complete (SC) medium containing 0.17% yeast nitrogen base (US Biological), 0.5% ammonium sulfate, 2 mM sodium hydroxide, and 0.07% SC supplement was used; SCD is SC containing 2% dextrose. SCD dropout medium lacking uracil was used in cells transformed with pYES2 plasmid, and SC with galactose lacking uracil was used to induce *YDC1* open reading frame in pYES2 plasmid for the overexpression studies. For all experiments, cells were treated during mid-log growth at 30°C. Heat stress was performed by shifting cells to a 39°C water bath after 45 min of pretreatment with myriocin (Sigma) or vehicle. Cultures were harvested by centrifugation at 3000*g* for 3 min and stored at −80°C. For spot tests, compounds required for specified treatments including glycerol, sodium chloride, acetic acid, caffeine, Congo red, hygromycin B, and Rose Bengal were purchased from Sigma. All compounds, including fatty acid (myristate or oleate) or vehicle (0.1% ethanol), were dissolved in medium by warming to 50°C for 10 min. After medium was re-equilibrated to room temperature, it was mixed with 2× agar at 50°C to make SC with 2% agar; 25 ml of medium was poured into 100-mm petri dishes. Solidified plates were dried for 20 min at 37°C before use. Mid-log cultures in SCD were diluted [OD_{600} (optical density at 600 nm), 0.3], and then 5 μl of four serial 1:10 dilutions was spotted and incubated at 30°C for 3 to 5 days.

Heat stress and ISP1 treatment

Cells grown to mid-log (OD_{600}, 0.6) from overnight cultures were pretreated with 5 μM ISP1 or vehicle (0.1% methanol) for 45 min, and then heat stress samples were shifted from 30° to 39°C for 15 min. Samples (100 ml) were divided into 10- and 90-ml aliquots for microarray and lipidomic analysis, respectively, and then harvested at room temperature by centrifugation at 3000*g* for 3 min and flash-frozen in a dry ice methanol bath.

Myristate treatment

Cells grown to mid-log (OD_{600}, 0.6) from overnight cultures were pretreated with 5 μM myriocin or vehicle (0.1% methanol) for 45 min and then treated with 1 mM myristate (Sigma) or fatty acid vehicle (0.05% ethanol) for 15 min. Samples (100 ml) were divided into 10- and 90-ml aliquots for microarray and lipidomic analysis, respectively, and then harvested at room temperature for 3 min and flash-frozen in a dry ice methanol bath.

Systematic perturbations and collection of lipidomic and microarray data

Yeast cells (JK9-3dα) were subjected to the following combinations of perturbations: (i) control condition; (ii) ISP1 treatment at 30°C; (iii) heat stress; (iv) heat stress plus ISP1 treatment; (v) control condition for fatty acid supplement experiment, 30°C in SC medium; (vi) myristate treatment at 30°C; and (vii) myristate plus ISP1 treatment at 30°C. Experiments were repeated three times under each of the above condition.

RNA was extracted from 10^8 cells with the hot acid phenol method (*39*). Synthesis of complementary DNA (cDNA), in vitro transcription labeling, and hybridization onto the Yeast2.0 chip were conducted with the Affymetrix GeneChip Kit.

Cells were grown, treated, and extracted, and total protein was measured, all according to (*40*), and relative lipid concentrations were quantified according to the method of (*41*) and normalized to total protein.

YDC1 experiments

Wild type (BY4741) or *ydc1*Δ was used to perform experiments. Growth conditions and heat stress were done as described above. To achieve *YDC1* overexpression, a BY4741 strain was transformed with pYES2 plasmid containing an open reading frame of *YDC1* under galactose promoter. For galactose induction, cells were harvested from a dextrose-containing medium by centrifugation at 3000*g* for 3 min; pellets were washed with sterile water, then inoculated into a galactose-containing medium, and grown for 6 hours before treatment with heat stress. After heat stress, cells were harvested by centrifugation, washed with sterile water, and centrifuged again. The pellets were snap-frozen in liquid nitrogen until ready for RNA extraction.

Quantitative real-time reverse transcription polymerase chain reaction

Total RNA was harvested with hot acid phenol method, described in *Short Protocols in Molecular Biology*, unit 13.10 (*42*). First-strand cDNA was produced as described previously (*43*). Real-time analysis was done with 7500 Real-Time PCR System (Life Technologies), and SYBR Green Supermix

protocol (Bio-Rad) was used to perform the analysis. Primers used in the reverse transcription polymerase chain reaction are *AFT1* forward primer (TCAAAAGCACACATTCCCTCA) and *AFT1* reverse primer (AACTTTAAATGCGTCCGACC). The expression of target genes was normalized to the expression of three reference genes: *RDN18*, *ALG9*, and *TAF10*. The primers are as follows: *RDN18*, CCATGGTTTCAACGGGTAACG (forward) and GCCTTCCTTGGATGTGGTAGCC (reverse); *ALG9*, CACGGATAGTGGCTTTGGTGAACAATTAC (forward) and TATGATTATTCTGGCAGCAGGAAAGAACTTGGG (reverse); *TAF10*, ATATTCCAGGATCAGGTCTTCCGTAGC (forward) and GTAGTCTTCTCATTCTGTTGATGTTGTTGTTG (reverse).

Ontology-based gene function analysis

Given a set of genes that are significantly correlated to a specific lipid species and their annotations in the form of the GO (*44*) (http://www.geneontology.org) terms, we aimed to group genes into nondisjoint subsets, such that each module contained genes with closely related GO annotations, and the overall function of the module was represented by a GO term that captured most of the semantic information of the original GO annotations of the genes. We represented genes and their annotations with a data structure referred to as GOGene graph (*29*, *45*). In such a graph, a node represents a GO term, and a directed edge between a pair of nodes reflects an "is a" (ISA) relationship between the GO terms, that is, parent term subsumes that of the child term. In addition, each node kept track of the genes it annotated; therefore, the graph contained information of both GO terms and genes. We constructed a canonical graph with all GO terms in the Biological Process namespace, according to the ontology definition from the GO consortium (http://www.geneontology.org). When given a set of genes and their annotations, we associated the genes to GO terms on the basis of their annotations, and then we trimmed leaf nodes that had no genes associated. This produced a subgraph in which leaf nodes were a subset of the original GO annotations associated with the genes of interest. Under such a setting, the task of finding functionally coherent gene modules can be achieved by grouping genes according to their annotations through collapsing GOGene graph in a manner that leads to minimal information loss, and we stopped merging when the P value of assessing the functional coherence of a gene module was equal or greater than 0.05 (*29*).

Microarray and data analysis

Affymetrix CEL files of the microarray experiments were processed with the "affy" package (v 1.24.2), and differential expression was assessed with the "limma" package (v 3.2.3) of the Bioconductor Suite (http://www.bioconductor.org/). The threshold for detecting differential expression was set at $P < 0.01$ and $q < 0.05$.

Consensus clustering of lipidomic data

The R implementation of the clusterCons (*20*) was downloaded from the CRAN (Comprehensive R Archive Network) (http://cran.r-project.org/web/packages/clusterCons/). Lipidomic data (32 species in 21 experimental conditions) were used as input for the program in multiple runs. For each lipid species, the concentration is normalized to a standard normal distribution (zero mean and unit SD). The partition around medoids (PAM) and K means algorithms were used as base clustering algorithms to run the ConsensusPlus algorithm. The cluster size (K) is set through a range (6 to 13) to explore optimal number of clusters to group the lipids.

Correlation analysis of ceramide concentrations and gene expression

The software for calculating maximal information coefficient was downloaded from http://www.exploredata.net/ (accessed December 2012), which was maintained by the authors of the report by Reshef *et al.* (*25*). The statistical significance of the MIC values was determined with the significance table provided by the authors at the threshold of $P < 0.01$. Because the authors only provide the P values for MIC values that are sufficiently large, it is not possible to perform false discovery correction of these P values using the q values (*26*) package in such setting.

The Pearson correlation analysis was performed with the standard R language package. The returned P values for all lipid-versus-gene pairs were further subjected to false discovery correction with the q value package. The significance threshold is set at $P \leq 0.01$ and $q \leq 0.05$.

SUPPLEMENTARY MATERIALS

www.sciencesignaling.org/cgi/content/full/6/299/rs14/DC1
Fig. S1. The effect of myristate on the lipidomic profile, including the effect on sphingoids.
Fig. S2. Validation of lipid-specific growth phenotypes in triplicate.
Table S1. Lipidomics data under all combinations of treatments (xlxs).
Table S2. Microarray data heat stress (xlxs).
Table S3. Microarray data under all combinations of treatments (xlxs).
Table S4. List of lipid-gene pairs showing significant association measured by MIC (xlxs).
Table S5. List of lipid-gene pairs showing significant Pearson correlations (xlxs).
Table S6. List of lipid-gene pairs showing significant associations measured using Bayesian regression (xlxs).
Table S7. All treatments tested for fatty acid–specific growth defects.
Table S8. Yeast strains used in this study.

REFERENCES AND NOTES

1. Y. A. Hannun, L. M. Obeid, Principles of bioactive lipid signalling: Lessons from sphingolipids. *Nat. Rev. Mol. Cell Biol.* **9**, 139–150 (2008).
2. T. Kolter, A view on sphingolipids and disease. *Chem. Phys. Lipids* **164**, 590–606 (2011).
3. Y. A. Hannun, L. M. Obeid, Many ceramides. *J. Biol. Chem.* **286**, 27855–27862 (2011).
4. T. D. Mullen, S. Spassieva, R. W. Jenkins, K. Kitatani, J. Bielawski, Y. A. Hannun, L. M. Obeid, Selective knockdown of ceramide synthases reveals complex interregulation of sphingolipid metabolism. *J. Lipid Res.* **52**, 68–77 (2011).
5. S. D. Spassieva, M. Rahmaniyan, J. Bielawski, C. J. Clarke, J. M. Kraveka, L. M. Obeid, Cell density-dependent reduction of dihydroceramide desaturase activity in neuroblastoma cells. *J. Lipid Res.* **53**, 918–928 (2012).
6. L. A. Cowart, M. Shotwell, M. L. Worley, A. J. Richards, D. J. Montefusco, Y. A. Hannun, X. Lu, Revealing a signaling role of phytosphingosine-1-phosphate in yeast. *Mol. Syst. Biol.* **6**, 349 (2010).
7. G. B. Wells, R. C. Dickson, R. L. Lester, Heat-induced elevation of ceramide in *Saccharomyces cerevisiae* via de novo synthesis. *J. Biol. Chem.* **273**, 7235–7243 (1998).
8. L. A. Cowart, Y. A. Hannun, Selective substrate supply in the regulation of yeast de novo sphingolipid synthesis. *J. Biol. Chem.* **282**, 12330–12340 (2007).
9. L. A. Cowart, Y. Okamoto, F. R. Pinto, J. L. Gandy, J. S. Almeida, Y. A. Hannun, Roles for sphingolipid biosynthesis in mediation of specific programs of the heat stress response determined through gene expression profiling. *J. Biol. Chem.* **278**, 30328–30338 (2003).
10. G. M. Jenkins, Y. A. Hannun, Role for de novo sphingoid base biosynthesis in the heat-induced transient cell cycle arrest of *Saccharomyces cerevisiae*. *J. Biol. Chem.* **276**, 8574–8581 (2001).
11. N. Matmati, H. Kitagaki, D. Montefusco, B. K. Mohanty, Y. A. Hannun, Hydroxyurea sensitivity reveals a role for *ISC1* in the regulation of G_2/M. *J. Biol. Chem.* **284**, 8241–8246 (2009).
12. L. A. Cowart, J. L. Gandy, B. Tholanikunnel, Y. A. Hannun, Sphingolipids mediate formation of mRNA processing bodies during the heat-stress response of *Saccharomyces cerevisiae*. *Biochem. J.* **431**, 31–38 (2010).
13. G. G. Guenther, E. R. Peralta, K. R. Rosales, S. Y. Wong, L. J. Siskind, A. L. Edinger, Ceramide starves cells to death by downregulating nutrient transporter proteins. *Proc. Natl. Acad. Sci. U.S.A.* **105**, 17402–17407 (2008).
14. L. A. Cowart, Y. Okamoto, X. Lu, Y. A. Hannun, Distinct roles for de novo versus hydrolytic pathways of sphingolipid biosynthesis in *Saccharomyces cerevisiae*. *Biochem. J.* **393**, 733–740 (2006).
15. J. Petschnigg, H. Wolinski, D. Kolb, G. n. Zellnig, C. F. Kurat, K. Natter, S. D. Kohlwein, Good fat, essential cellular requirements for triacylglycerol synthesis to maintain membrane homeostasis in yeast. *J. Biol. Chem.* **284**, 30981–30993 (2009).
16. D. A. Toke, C. E. Martin, Isolation and characterization of a gene affecting fatty acid elongation in *Saccharomyces cerevisiae*. *J. Biol. Chem.* **271**, 18413–18422 (1996).
17. W. Al-Feel, J. C. DeMar, S. J. Wakil, A *Saccharomyces cerevisiae* mutant strain defective in acetyl-CoA carboxylase arrests at the G_2/M phase of the cell cycle. *Proc. Natl. Acad. Sci. U.S.A.* **100**, 3095–3100 (2003).

18. N. Matmati, A. Metelli, K. Tripathi, S. Yan, B. K. Mohanty, Y. A. Hannun, Identification of $c_{18:1}$-phytoceramide as the candidate lipid mediator for hydroxyurea resistance in yeast. *J. Biol. Chem.* **288**, 17272–17284 (2013).
19. S. Monti, P. Tamayo, J. Mesirov, T. Golub, Consensus clustering: A resampling-based method for class discovery and visualization of gene expression microarray data. *Mach. Learn.* **52**, 91–118 (2003).
20. T. I. Simpson, J. D. Armstrong, A. P. Jarman, Merged consensus clustering to assess and improve class discovery with microarray data. *BMC Bioinformatics* **11**, 590 (2010).
21. C. J. Mousley, K. Tyeryar, K. E. Ile, G. Schaaf, R. L. Brost, C. Boone, X. Guan, M. R. Wenk, V. A. Bankaitis, *Trans*-Golgi network and endosome dynamics connect ceramide homeostasis with regulation of the unfolded protein response and TOR signaling in yeast. *Mol. Biol. Cell* **19**, 4785–4803 (2008).
22. R. C. Dickson, C. Sumanasekera, R. L. Lester, Functions and metabolism of sphingolipids in *Saccharomyces cerevisiae*. *Prog. Lipid Res.* **45**, 447–465 (2006).
23. D. J. Klionsky, H. Abeliovich, P. Agostinis, D. K. Agrawal, G. Aliev, D. S. Askew, M. Baba, E. H. Baehrecke, B. A. Bahr, A. Ballabio, B. A. Bamber, D. C. Bassham, E. Bergamini, X. Bi, M. Biard-Piechaczyk, J. S. Blum, D. E. Bredesen, J. L. Brodsky, J. H. Brumell, U. T. Brunk, W. Bursch, N. Camougrand, E. Cebollero, F. Cecconi, Y. Chen, L. S. Chin, A. Choi, C. T. Chu, J. Chung, P. G. Clarke, R. S. Clark, S. G. Clarke, C. Clavé, J. L. Cleveland, P. Codogno, M. I. Colombo, A. Coto-Montes, J. M. Cregg, A. M. Cuervo, J. Debnath, F. Demarchi, P. B. Dennis, P. A. Dennis, V. Deretic, R. J. Devenish, F. Di Sano, J. F. Dice, M. Difiglia, S. Dinesh-Kumar, C. W. Distelhorst, M. Djavaheri-Mergny, F. C. Dorsey, W. Dröge, M. Dron, W. A. Dunn Jr., M. Duszenko, N. T. Eissa, Z. Elazar, A. Esclatine, E. L. Eskelinen, L. Fésüs, K. D. Finley, J. M. Fuentes, J. Fueyo, K. Fujisaki, B. Galliot, F. B. Gao, D. A. Gewirtz, S. B. Gibson, A. Gohla, A. L. Goldberg, R. Gonzalez, C. González-Estévez, S. Gorski, R. A. Gottlieb, D. Häussinger, Y. W. He, K. Heidenreich, J. A. Hill, M. Høyer-Hansen, X. Hu, W. P. Huang, A. Iwasaki, M. Jäättelä, W. T. Jackson, X. Jiang, S. Jin, T. Johansen, J. U. Jung, M. Kadowaki, C. Kang, A. Kelekar, D. H. Kessel, J. A. Kiel, H. P. Kim, A. Kimchi, T. J. Kinsella, K. Kiselyov, K. Kitamoto, E. Knecht, M. Komatsu, E. Kominami, S. Kondo, A. L. Kovács, G. Kroemer, C. Y. Kuan, R. Kumar, M. Kundu, J. Landry, M. Laporte, W. Le, H. Y. Lei, M. J. Lenardo, B. Levine, A. Lieberman, K. L. Lim, F. C. Lin, W. Liou, L. F. Liu, G. Lopez-Berestein, C. López-Otín, B. Lu, K. F. Macleod, W. Malorni, W. Martinet, K. Matsuoka, J. Mautner, A. J. Meijer, A. Meléndez, P. Michels, G. Miotto, W. P. Mistiaen, N. Mizushima, B. Mograbi, I. Monastyrska, M. N. Moore, P. I. Moreira, Y. Moriyasu, T. Motyl, C. Münz, L. O. Murphy, N. I. Naqvi, T. P. Neufeld, I. Nishino, R. A. Nixon, T. Noda, B. Nürnberg, M. Ogawa, N. L. Oleinick, L. J. Olsen, B. Ozpolat, S. Paglin, G. E. Palmer, I. Papassideri, M. Parkes, D. H. Perlmutter, G. Perry, M. Piacentini, R. Pinkas-Kramarski, M. Prescott, T. Proikas-Cezanne, N. Raben, A. Rami, F. Reggiori, B. Rohrer, D. C. Rubinsztein, K. M. Ryan, J. Sadoshima, H. Sakagami, Y. Sakai, M. Sandri, C. Sasakawa, M. Sass, C. Schneider, P. O. Seglen, O. Seleverstov, J. Settleman, J. J. Shacka, I. M. Shapiro, A. Sibirny, E. C. Silva-Zacarin, H. U. Simon, C. Simone, A. Simonsen, M. A. Smith, K. Spanel-Borowski, V. Srinivas, M. Steeves, H. Stenmark, P. E. Stromhaug, C. S. Subauste, S. Sugimoto, D. Sulzer, T. Suzuki, M. S. Swanson, I. Tabas, F. Takeshita, N. J. Talbot, Z. Tallóczy, K. Tanaka, K. Tanaka, I. Tanida, G. S. Taylor, J. P. Taylor, A. Terman, G. Tettamanti, C. B. Thompson, M. Thumm, A. M. Tolkovsky, S. A. Tooze, R. Truant, L. V. Tumanovska, Y. Uchiyama, T. Ueno, N. L. Uzcátegui, I. van der Klei, E. C. Vaquero, T. Vellai, M. W. Vogel, H. G. Wang, P. Webster, J. W. Wiley, Z. Xi, G. Xiao, J. Yahalom, J. M. Yang, G. Yap, X. M. Yin, T. Yoshimori, L. Yu, Z. Yue, M. Yuzaki, O. Zabirnyk, X. Zheng, X. Zhu, R. L. Deter, Guidelines for the use and interpretation of assays for monitoring autophagy in higher eukaryotes. *Autophagy* **4**, 151–175 (2008).
24. M. Liu, C. Huang, S. R. Polu, R. Schneiter, A. Chang, Regulation of sphingolipid synthesis via Orm1 and Orm2 in yeast. *J. Cell Sci.* **125**, 2428–2435 (2012).
25. D. N. Reshef, Y. A. Reshef, H. K. Finucane, S. R. Grossman, G. McVean, P. J. Turnbaugh, E. S. Lander, M. Mitzenmacher, P. C. Sabeti, Detecting novel associations in large data sets. *Science* **334**, 1518–1524 (2011).
26. J. Storey, The positive false discovery rate: A Bayesian interpretation and the *q*-value. *Ann. Statist.* **31**, 2013–2035 (2003).
27. P. Good, *Permutation Tests: A Practical Guide to Resampling Methods for Testing Hypotheses* (Springer, Berlin, 1994).
28. J. Friedman, T. Hastie, R. Tibshirani, Regularization paths for generalized linear models via coordinate descent. *J. Stat. Softw.* **33**, 1–22 (2010).
29. V. Chen, X. Lu, Conceptualization of molecular findings by mining gene annotations. *BMC Proc.*, in press.
30. C. Mao, R. Xu, A. Bielawska, L. M. Obeid, Cloning of an alkaline ceramidase from *Saccharomyces cerevisiae*. An enzyme with reverse (CoA-independent) ceramide synthase activity. *J. Biol. Chem.* **275**, 6876–6884 (2000).
31. M. Sambade, M. Alba, A. M. Smardon, R. W. West, P. M. Kane, A genomic screen for yeast vacuolar membrane ATPase mutants. *Genetics* **170**, 1539–1551 (2005).
32. G. Giaever, A. M. Chu, L. Ni, C. Connelly, L. Riles, S. Véronneau, S. Dow, A. Lucau-Danila, K. Anderson, B. André, A. P. Arkin, A. Astromoff, M. El-Bakkoury, R. Bangham, R. Benito, S. Brachat, S. Campanaro, M. Curtiss, K. Davis, A. Deutschbauer, K. D. Entian, P. Flaherty, F. Foury, D. J. Garfinkel, M. Gerstein, D. Gotte, U. Güldener, J. H. Hegemann, S. Hempel, Z. Herman, D. F. Jaramillo, D. E. Kelly, S. L. Kelly, P. Kötter, D. LaBonte, D. C. Lamb, N. Lan, H. Liang, H. Liao, L. Liu, C. Luo, M. Lussier, R. Mao, P. Menard, S. L. Ooi, J. L. Revuelta, C. J. Roberts, M. Rose, P. Ross-Macdonald, B. Scherens, G. Schimmack, B. Shafer, D. D. Shoemaker, S. Sookhai-Mahadeo, R. K. Storms, J. N. Strathern, G. Valle, M. Voet, G. Volckaert, C. Y. Wang, T. R. Ward, J. Wilhelmy, E. A. Winzeler, Y. Yang, G. Yen, E. Youngman, K. Yu, H. Bussey, J. D. Boeke, M. Snyder, P. Philippsen, R. W. Davis, M. Johnston, Functional profiling of the *Saccharomyces cerevisiae* genome. *Nature* **418**, 387–391 (2002).
33. N. Mira, M. Teixeira, I. Sá-Correia, Adaptative response and tolerance to weak acid stress in *Saccharomyces cerevisiae*: A genome-wide view. *OMICS* **14**, 525–540 (2010).
34. P. Motshwene, R. Karreman, G. Kgari, W. Brandt, G. Lindsey, LEA (late embryonic abundant)-like protein Hsp 12 (heat-shock protein 12) is present in the cell wall and enhances the barotolerance of the yeast *Saccharomyces cerevisiae*. *Biochem. J.* **377**, 769–774 (2004).
35. R. J. Karreman, G. G. Lindsey, Modulation of Congo-red-induced aberrations in the yeast Saccharomyces cerevisiae by the general stress response protein Hsp12p. *Can. J. Microbiol.* **53**, 1203–1210 (2007).
36. S. Li, S. Dean, Z. Li, J. Horecka, R. J. Deschenes, J. S. Fassler, The eukaryotic two-component histidine kinase Sln1p regulates *OCH1* via the transcription factor, Skn7p. *Mol. Biol. Cell* **13**, 412–424 (2002).
37. K. Brombacher, B. B. Fischer, K. Rüfenacht, R. I. L. Eggen, The role of Yap1p and Skn7p-mediated oxidative stress response in the defence of *Saccharomyces cerevisiae* against singlet oxygen. *Yeast* **23**, 741–750 (2006).
38. C. Glymour, G. Cooper, *Computation, Causation, and Discovery* (MIT Press, Cambridge, MA, 1999).
39. M. A. Collart, S. Oliviero, Preparation of yeast RNA, in *Current Protocols in Molecular Biology* (John Wiley & Sons Inc., New York, 1993), pp. 13.12.1–13.12.5.
40. D. J. Montefusco, B. Newcomb, J. L. Gandy, S. E. Brice, N. Matmati, L. A. Cowart, Y. A. Hannun, Sphingoid bases and the serine catabolic enzyme *CHA1* define a novel feedforward/feedback mechanism in the response to serine availability. *J. Biol. Chem.* **287**, 9280–9289 (2012).
41. J. Bielawski, Z. M. Szulc, Y. A. Hannun, A. Bielawska, Simultaneous quantitative analysis of bioactive sphingolipids by high-performance liquid chromatography-tandem mass spectrometry. *Methods* **39**, 82–91 (2006).
42. F. M. Ausubel, *Short Protocols in Molecular Biology: A Compendium of Methods from Current Protocols in Molecular Biology* (Wiley, New York, 2002).
43. H. Kitagaki, L. A. Cowart, N. Matmati, D. Montefusco, J. Gandy, S. V. de Avalos, S. A. Novgorodov, J. Zheng, L. M. Obeid, Y. A. Hannun, *ISC1*-dependent metabolic adaptation reveals an indispensable role for mitochondria in induction of nuclear genes during the diauxic shift in *Saccharomyces cerevisiae*. *J. Biol. Chem.* **284**, 10818–10830 (2009).
44. M. Ashburner, C. A. Ball, J. A. Blake, D. Botstein, H. Butler, J. M. Cherry, A. P. Davis, K. Dolinski, S. S. Dwight, J. T. Eppig, M. A. Harris, D. P. Hill, L. Issel-Tarver, A. Kasarskis, S. Lewis, J. C. Matese, J. E. Richardson, M. Ringwald, G. M. Rubin, G. Sherlock, Gene Ontology: Tool for the unification of biology. The Gene Ontology Consortium. *Nat. Genet.* **25**, 25–29 (2000).
45. B. Muller, A. J. Richards, B. Jin, X. Lu, GOGrapher: A Python library for GO graph representation and analysis. *BMC Res. Notes* **2**, 122 (2009).

Acknowledgments: We acknowledge the Medical University of South Carolina (MUSC) Lipidomics facility as well as the MUSC ProteoGenomics facility for their services. We would also like to thank L. A. Cowart for commenting on the manuscript and C. Mao for providing the plasmid overexpressing *YDC1* and for his suggestions and comments. **Funding:** This work is partially supported by NIH grants R01LM 010144, R01LM011155 (X.L.), R01LM010020 (G.F.C.), and R01GM063265 (Y.A.H.). **Author contributions:** Y.A.H. and X.L. conceived and directed the study; D.J.M., N.M., and B.N. performed yeast experiments, lipidomics, microarray data collection, and yeast validation experiments; L.C., S.L., G.F.C., and X.L. performed data analysis and modeling; and D.J.M., L.C., N.M., X.L., and Y.A.H. drafted and edited the manuscript. **Competing interests:** The authors declare that they have no competing interests. **Data and materials availability:** Data are available as supplementary tables and from http://www.dbmi.pitt.edu/publications/YeastCeramideSignaling.

Submitted 15 July 2013
Accepted 10 October 2013
Final Publication 29 October 2013
10.1126/scisignal.2004515
Citation: D. J. Montefusco, L. Chen, N. Matmati, S. Lu, B. Newcomb, G. F. Cooper, Y. A. Hannun, X. Lu, Distinct signaling roles of ceramide species in yeast revealed through systematic perturbation and systems biology analyses. *Sci. Signal.* **6**, rs14 (2013).

Distinct Signaling Roles of Ceramide Species in Yeast Revealed Through Systematic Perturbation and Systems Biology Analyses

David J. Montefusco, Lujia Chen, Nabil Matmati, Songjian Lu, Benjamin Newcomb, Gregory F. Cooper, Yusuf A. Hannun and Xinghua Lu (October 29, 2013)

Science Signaling **6** (299), rs14. [doi: 10.1126/scisignal.2004515]